Available online at www.sciencedirect.com
SCIENCE DIRECT®
Optics Communications 233 (2004) 311–322
OPTICS COMMUNICATIONS
www.elsevier.com/locate/optcom

Effect of a depth attenuated refractive index profile in the angular responses of the efficiency of higher orders in volume gratings recorded in a PVA/acrylamide photopolymer

C. Neipp [a,*], J.T. Sheridan [b], S. Gallego [c], M. Ortuño [c], A. Márquez [a], I. Pascual [c], A. Beléndez [a]

[a] Departamento de Física, Ingeniería de Sistemas y Teoría de la Señal, Universidad de Alicante, Ap. 99, E-03080 Alicante, Spain
[b] Departament of Electronic and Electrical Engineering, University College Dublin, Belfield, Dublin 4, Ireland
[c] Departamento Interuniversitario de Óptica, Universidad de Alicante, Apartado 99, E-03080 Alicante, Spain

Received 1 July 2003; received in revised form 27 January 2004; accepted 27 January 2004

Abstract

A great deal of research has been carried out recently in the field of volume gratings recorded in photopolymer material. The existence of different models that predict the mechanism of hologram formation inside photopolymers, has increased the possibilities of an accurate understanding of the processes involved inside photopolymers during the exposure process. A great deal of experimental research has been done, in order to test the theoretical assumptions. Nonetheless, there is little quantitative data available about higher harmonics components of the refractive index. This is due to the fact that, apart from a few works, Kogelnik's coupled wave theory has been used to fit the temporal evolution of the diffraction efficiency of the first order. The use of this theory does not allow us to obtain information about higher orders and consequently about the higher harmonics in the refractive index. In this paper we apply an algorithm based in the rigorous coupled wave theory to reproduce the angular response curves of the different orders that propagate inside the hologram. This study will be done for attenuated in depth grating profiles. Experimental data for the angular responses of the first and second orders, centered at first and second on Bragg angular replay conditions, will be examined. The experimental data provided will demonstrate that attenuation occurs inside the hologram during the recording step, most probably because of Beer's Law. The information provided in this work is significant, since future theoretical models of grating formation in photopolymers should explain this behaviour.

PACS: 42.40; 42.70.L; 42.40.E

Keywords: Holography; Volume holograms; Holographic recording materials; Photopolymers; Diffraction gratings

* Corresponding author. Tel.: +34-6-5903682/3651; fax: +34-6-5909750/3464.
E-mail address: cristian@disc.ua.es (C. Neipp).

0030-4018/$ - see front matter © 2004 Elsevier B.V. All rights reserved.
doi:10.1016/j.optcom.2004.01.064

1. Introduction

The use of the rigorous coupled wave theory (RCWT) to explain how the electromagnetic field propagates inside different periodic structures has been an important topic in recent years. The method was first described by Moharam and Gaylord [1] for use in modelling planar dielectric gratings. However, since then, Moharam, Gaylord and their co-workers [2–6] have applied the RCWT analysis to study many different types of periodic structures. The RCWT has also been used by Kamiya [7] to study practical volume holograms. In addition the RCWT has been successfully applied to the study of diffractive optical elements [8] and also of photonic band structures [9].

The first algorithm proposed by Moharam and Gaylord [1] encountered some numerical difficulties. The retention of high positive eigenvalues of the matrix of constant coefficients, describing the differential equations in the periodic structure, could lead to numerical instabilities. In addition, the original algorithm demonstrated poor convergence for TM polarization. This fact led to a series of papers with the aim of eliminating these difficulties. The same authors formulated a stable algorithm presenting no numerical instabilities [6]. This new formulation also allows results for high thickness to be calculated. As will be seen this is an important fact when applying the RCWT to photopolymer materials.

Parallel to the improvements in the RCWT method, the application and models of photopolymer materials for the recording of high quality diffraction elements has also seen important developments. New theoretical models that permit a deeper understanding of the mechanism of hologram formation in photopolymer materials have been proposed. Since the polymerisation driven diffusion (PDD) model proposed by Zhao et al. [10] several new models have been presented which give a clearer understanding of the hologram formation mechanisms in photopolymers [10–19]. For example, the non-local polymerisation driven diffusion (NPDD) model proposed by Sheridan and co-workers, explains more experimental facts, such as the cut-off of diffraction efficiency for high spatial frequencies. All PDD models predict the existence of higher harmonics in the refractive index. Nonetheless, the usual method to check their validity has been the use of the first order two wave analytical formula derived by Kogelnik [20]. It has estimated in a recent paper by Wu and Glytsis [21] that the use of Kogelnik's theory can lead to worst case errors as high as 30% in the value of the first harmonic component of the refractive index, n_1, compared to the RCWT method.

In a previous paper [22] we have applied the RCWT method to predict the angular response curve of the efficiency of the second order, in this way the higher harmonics in the refractive index recorded in the photopolymer have been obtained. It is clear, therefore, that the use of electromagnetic models allowing for more than two orders, to obtain information of the mechanisms of hologram formation in photopolymers is necessary.

In this work we implement an algorithm based on the stable formulation of the RCWT proposed by Moharam et al. [6] to examine the attenuation of the refractive index distribution inside photopolymer materials of high thickness. Apart from the work by Blaya et al. [23] none of the diffusion models consider this attenuation of the profile with thickness. This work incorporated the effects of the attenuation in the efficiency curves of the first order by using Uchida's first order two wave analytical expressions [24]. In this work we extend the study to higher orders and will present experimental data of angular responses of the efficiency of the second order to prove that an attenuated grating profile is stored in the holograms formed in PVA/acrylamide based photopolymers.

2. Rigorous coupled wave method for periodic attenuated profiles

2.1. Rigorous coupled wave equations

In this section the differential equations that govern the behavior of the different diffracted orders propagating inside a transmission diffraction grating will be derived using the RCWT formalism [6]. A more general treatment for the analysis of

single cascaded anisotropic gratings can be found in [25].

The profile of the dielectric permittivity will only be supposed to vary in the x and z directions, therefore a planar diffraction grating is studied. The study will also be restricted to the case of unslanted gratings so the dependence of dielectric permittivity with x, z will be assumed to be in the form

$$\varepsilon(x,z) = \sum_h \varepsilon_h(z) \exp[\mathrm{j}hKx], \tag{1}$$

K is the modulus of the grating vector, which is related to the period of the interference fringes, Λ, as follows

$$K = 2\pi/\Lambda. \tag{2}$$

To include the effect of an attenuated grating profile recorded in the photopolymer material each Fourier component of the permittivity will be expressed as a function of z as

$$\varepsilon_h(z) = \varepsilon_{h,0} \exp[-\alpha z], \tag{3}$$

where $\varepsilon_{h,0}$ are the initial values (at $z = 0$) of the harmonic components of the dielectric permittivity.

In order to apply the RCWT to obtain the efficiency of the different orders we will study a periodic structure such as that in Fig. 1. All the periodic structure (medium 2), the hologram, is supposed to be embedded between two media, medium 1 and medium 3. The hologram will be divided in G different sub-gratings of thickness d_g each. The total thickness of the hologram, d, can be obtained as the sum of the thickness of the different sub-gratings

$$d = \sum_{g=1}^{G} d_g, \tag{4}$$

where G is the number of gratings retained.

Each sub-grating will be supposed to have a periodic dielectric permittivity of the form

$$\varepsilon_g(x) = \sum_h \varepsilon_{g,h} \exp[\mathrm{j}hKx], \tag{5}$$

$\varepsilon_{g,h}$ is the hth Fourier component of the relative permittivity in the grating region g, which can be expressed as

$$\varepsilon_{g,h} = \varepsilon_{0,h} \exp\left[-\alpha \sum_{g'=1}^{g} d_{g'}\right]. \tag{6}$$

We will also study the case of TE polarization, so the waves propagate in the xz plane, with the electric field polarized in the y direction.

If a unit amplitude plane wave impinges onto the hologram from medium 1, the electric field in mediums 1 and 3 can be expressed as:

$$E_1 = \exp[-\mathrm{j}(k_{x0}x + k_{z0}z)] + \sum_i R_i \exp[-\mathrm{j}(k_{xi}x - k_{zi1}z)], \tag{7}$$

$$E_3 = \sum_i T_i \exp\{-\mathrm{j}[k_{xi}x + k_{zi3}(z-d)]\}, \tag{8}$$

where $k_{x0} = k_0 \varepsilon_1^{1/2} \sin\theta$, $k_{z0} = k_0 \varepsilon_1^{1/2} \cos\theta$, $k_0 = 2\pi/\lambda_0$, θ is the angle of incidence in medium 1, λ_0 is the free-space wavelength, ε_1 is the relative permittivity of medium 1, R_i is the amplitude of the ith order backward-diffracted wave and T_i is the amplitude of the ith order forward-diffracted wave. k_{xi} is determined from the Floquet condition

$$k_{xi} = k_{x0} - iK, \tag{9}$$

where the z components of the propagation vectors for the ith orders are

$$k_{zil} = (k_0^2 \varepsilon_l - k_{xi}^2)^{1/2}, \quad l = 1, 3. \tag{10}$$

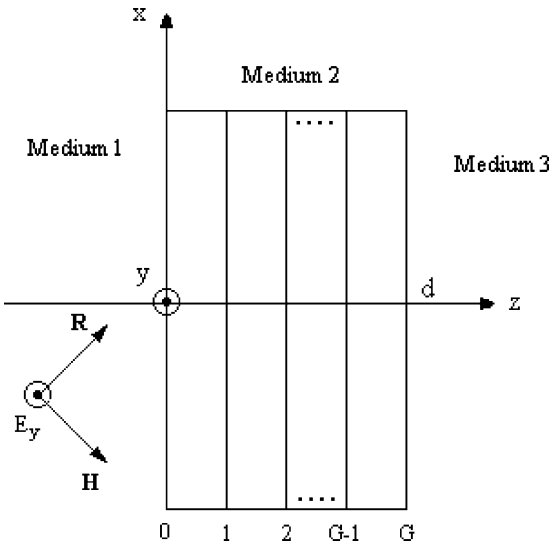

Fig. 1. Holographic grating structure.

To calculate the electric and magnetic field inside medium 2, Maxwell equations must be solved for each sub-grating. If $\boldsymbol{E}_g$ and $\boldsymbol{H}_g$ stand for the electric and magnetic field in the sub-grating g. Maxwell equations in the sub-grating g are:

$$\nabla \times \boldsymbol{E}_g = -\mathrm{j}\omega\mu_0 \boldsymbol{H}_g, \tag{11}$$

$$\nabla \times \boldsymbol{H}_g = \mathrm{j}\omega\varepsilon_0 \varepsilon_g(x,z)\boldsymbol{E}_g, \tag{12}$$

ε_0 and μ_0 are the vacuum dielectric permittivity and magnetic permeability, respectively and ω is the angular optical frequency of the electromagnetic wave in vacuum.

In sub-grating g, the tangential electric (y component) and magnetic (x component) fields may be expressed as:

$$E_{g,y} = \sum_i S_{g,yi}(z)\exp(-\mathrm{j}k_{xi}x), \tag{13}$$

$$H_{g,x} = -\mathrm{j}\left(\frac{\varepsilon_0}{\mu_0}\right)^{1/2} \sum_i U_{g,xi}(z)\exp(-\mathrm{j}k_{xi}x). \tag{14}$$

By substituting Eqs. (13) and (14) and Eq. (5) into Maxwell's equations the following set of coupled equations can be derived:

$$\frac{\partial S_{g,yi}}{\partial z} = k_0 U_{g,xi}, \tag{15}$$

$$\frac{\partial U_{g,xi}}{\partial z} = \left(\frac{k_{xi}^2}{k_0}\right) S_{g,yi} - k_0 \sum_p \varepsilon_{g,(i-p)} S_{g,yp}. \tag{16}$$

The amplitudes $S_{g,yi}$ and $U_{g,xi}$, can be obtained after solving Eqs. (15) and (16) by using the formalism in [6].

Eqs. (15) and (16) can be reduced to a set of second order coupled wave equations, which in matrix form can be expressed as

$$[\partial^2 S_{g,y}/\partial^2 (z')^2] = [A_g][S_{g,y}], \tag{17}$$

where $z' = k_0 z$.

$S_{g,y}$ is a column vector with the ith row being $S_{g,yi}$ and A_g is a matrix which can be obtained in the form

$$A_g = K_{g,x}^2 - E_g, \tag{18}$$

where E_g is the matrix formed by the permittivity harmonic components, with the i,p element being equal to $\varepsilon_{g,(i-p)}$ and $K_{g,x}$ is a diagonal matrix, with the ith diagonal elements being equal to $k_{g,xi}/k_0$.

The solutions of Eq. (17) are expressed in terms of the eigenvalues and eigenvectors of matrix A_g:

$$S_{g,yi}(z) = \sum_{m=1}^{n} w_{g,i,m}\left\{ c_{g,m}^{+}\exp\left[-k_0 q_{g,m}\left(z - \sum_{g'=1}^{g-1} d_{g'}\right)\right] + c_{g,m}^{-}\exp\left[k_0 q_{g,m}\left(z - \sum_{g'=1}^{g} d_{g'}\right)\right]\right\}, \tag{19}$$

$$U_{g,xi}(z) = \sum_{m=1}^{n} v_{g,i,m}\left\{ -c_{g,m}^{+}\exp\left[-k_0 q_{g,m}\left(z - \sum_{g'=1}^{g-1} d_{g'}\right)\right] + c_{g,m}^{-}\exp\left[k_0 q_{g,m}\left(z - \sum_{g'=1}^{g} d_{g'}\right)\right]\right\}. \tag{20}$$

If W_g is the matrix composed of the eigenvectors of matrix A_g, Q_g is a diagonal matrix composed of the positive square root of the eigenvalues of the matrix A_g and V_g is the matrix $V_g = W_g Q_g$. The quantities $w_{g,i,m}$ and $v_{g,i,m}$ represent the ith row mth column elements of matrixes W_g and V_g, respectively, whereas $q_{g,m}$ is the mth element in the diagonal of matrix Q_g.

In order to obtain the values of the $2 \times N$ arbitrary constants in each subgrating, where N is the number of orders retained, the boundary conditions for the electric and magnetic field must be imposed:

1. At the first boundary between the first medium and the first sub-grating; $z = 0$; Phase matching tangential $\boldsymbol{E}$ gives

$$\delta_{i0} + R_i = \sum_{m=1}^{n} w_{g,i,m} \times [c_{1,m}^{+} + c_{1,m}^{-}\exp(-k_0 q_{g,m} d_1)], \tag{21}$$

and for tangential $\boldsymbol{H}$:

$$\mathrm{j}\delta_{i0}[k_{x0} - k_{1,zi}R_i]/k_0 = \sum_{m=1}^{n} v_{1,i,m}[c_{1,m}^{+} - c_{1,m}^{-}\exp(-k_0 q_{1,m} d_1)]. \tag{22}$$

2. At the boundaries between two different subgratings (interface $(g-1)-g$), $z = \sum_{g'=1}^{g-1} d_{g'}$.

Tangential $\boldsymbol{E}$:

$$\sum_{m=1}^{n} w_{g-1,i,m}[c^{+}_{g-1,m}\exp(-k_0 q_{g,m} d_{g-1}) + c^{-}_{g-1,m}] = \sum_{m=1}^{n} w_{g,i,m}[c^{+}_{g,m} + c^{-}_{g,m}\exp(-k_0 q_{g,m} d_{g-1})]. \tag{23}$$

Tangential $\boldsymbol{H}$:

$$\sum_{m=1}^{n} v_{g-1,i,m}[c^{+}_{g-1,m}\exp(-k_0 q_{g,m} d_{g-1}) - c^{-}_{g-1,m}] = \sum_{m=1}^{n} v_{g,i,m}[c^{+}_{g,m} - c^{-}_{g,m}\exp(-k_0 q_{g,m} d_{g-1})]. \tag{24}$$

3. Finally phase matching $\boldsymbol{E}$ and $\boldsymbol{H}$ at the last boundary between the grating structure (medium 2) and medium 3; $z = \sum_{g'=1}^{G} d_{g'} = d$:

$$\sum_{m=1}^{n} w_{G,i,m}[c^{+}_{G,m}\exp(-k_0 q_{G,m} d_G) + c^{-}_{G,m}] = T_i, \tag{25}$$

$$\sum_{m=1}^{n} v_{G,i,m}[c^{+}_{G,m}\exp(-k_0 q_{g,m} d_G) - c^{-}_{G,m}] = \mathrm{j}(k_{2,zi}/k_0) T_i. \tag{26}$$

The diffraction efficiencies for the different orders are expressed as:

$$DE_{ri} = R_i R_i^{*}\mathrm{Re}\left(\frac{k_{1,zi}}{k_{z0}}\right), \tag{27}$$

$$DE_{ti} = T_i T_i^{*}\mathrm{Re}\left(\frac{k_{3zi}}{k_{z0}}\right). \tag{28}$$

Eqs. (21)–(26) form a set of equations with an equal number of unknowns. Therefore the values of coefficients $c^{-}_{g,m}$ and $c^{+}_{g,m}$ for each subgrating can be determined, and from Eq. (25) the values of the transmitted wave amplitudes in medium can also be calculated. Nonetheless, if typical inversion matrix algorithms are used to solve the set of Eqs. (21)–(26) of constant coefficients, numerical unstabilities emerge as a consequence of zero elements in the Eqs. (21)–(26) due to high positive eigenvalues. Therefore, in the next section, we propose another method to solve the problem only taking into account the transmitted waves inside the periodic medium.

2.2. Method of solution based on transmitted waves through the grating structure

The basis of the method consists in supposing that each sub-grating can be studied independently, applying the RCWT method to each and neglecting all reflected orders, the transmitted waves generated after passing each sub-grating enter in the next sub-grating. Thus, the possible reflected waves coming back to a grating due to the next one are disregarded. It is important to notice that this is a quite good approximation for volume unslanted gratings assuming there are no abrupt changes of refractive index inside the grating, which is acceptable in the case we are studying. It should be said that the method proposed was tested with the RCWT method (no attenuation assumed) with three, five and seven orders, also 3, 5 and 7 layers were used, and the results were consistent.

The electric field incident on subgrating g can be expressed as

$$E_{g-1} = \sum_i T_{g-1,i}\exp\left\{-\mathrm{j}\left[k_{xi}x + k_{gzi}\left(z - \sum_{g'=1}^{g-1} d_{g'}\right)\right]\right\}, \tag{29}$$

while the electric field that emerges from grating g is

$$E_g = \sum_i T_{g,i}\exp\left\{-\mathrm{j}\left[k_{xi}x + k_{gzi}\left(z - \sum_{g'=1}^{g} d_{g'}\right)\right]\right\}. \tag{30}$$

Now matching the tangential components of the electric field at $z = \sum_{g'=1}^{g-1} d_{g'}$ gives

$$T_{g-1,i} = \sum_{m=1}^{n} w_{g,i,m}[c^{+}_{g,m} + c^{-}_{g,m}\exp(-k_0 q_{g,m} d_{g-1})]. \tag{31}$$

At the interface $z = \sum_{g'=1}^{g} d_{g'}$

Tangential **E**:

$$\sum_{m=1}^{n} w_{g,i,m}[c^{+}_{g,m}\exp(-k_0 q_{g,m} d_g) + c^{-}_{g,m}] = T_{g,i}. \tag{32}$$

Tangential **H**:

$$\sum_{m=1}^{n} v_{g,i,m}[c_{g,m}^{+}\exp(-k_0 q_{g,m} d_g) - c_{g,m}^{-}] = \mathrm{j}(k_{g+1,zi}/k_0)T_{g,i}, \quad (33)$$

where

$$k_{g,zi} = (k_0^2 \varepsilon_{g,0} - k_{xi}^2)^{1/2}. \quad (34)$$

The algorithm used will be described as follows:

1. $c_{1,m}^{-}$ and $c_{1,m}^{+}$ are calculated in the first subgrating, $g = 1$:

   By eliminating R_i from Eqs. (21) and (22) the following equation in terms of the $2 \times N$ unknown constants $c_{1,m}^{-}$ and $c_{1,m}^{+}$ in the first sub-grating can be obtained

$$\begin{aligned}\mathrm{j}\delta_{i0}[k_{x0} + k_{1,zi}]/k_0 &= \sum_{m=1}^{n} [v_{1,i,m} + \mathrm{j}(k_{1,zi}/k_0)w_{1,i,m}]c_{1,m}^{+} \\ &+ [-v_{1,i,m} + \mathrm{j}(k_{1,zi}/k_0)w_{1,i,m}]c_{1,m}^{-} \\ &\times \exp(-k_0 q_{1,m} d_1)]. \end{aligned} \quad (35)$$

   Also by eliminating $T_{1,i}$ from Eqs. (32) and (33) the following equation can be obtained

$$\begin{aligned}0 = \sum_{m=1}^{n} &[-v_{1,i,m} + \mathrm{j}(k_{1,zi}/k_0)w_{1,i,m}]c_{1,m}^{+}\exp(-k_0 q_{1,m} d_1) \\ &+ [v_{1,i,m} + \mathrm{j}(k_{1,zi}/k_0)w_{1,i,m}]c_{1,m}^{-}]. \end{aligned} \quad (36)$$

   Eqs. (35) and (36) form a set of $2 \times N$ equations with $2 \times N$ unknowns and the values of $c_{1,m}^{-}$ and $c_{1,m}^{+}$ are calculated. By using Eq. (32) the values of $T_{1,i}$ are calculated.
2. Once the values of $T_{1,i}$ are known, these can be used in Eq. (31). With the aid of Eqs. (32) and (33) the values of $c_{2,m}^{-}$ and $c_{2,m}^{+}$ can also be calculated and finally with the aid of Eq. (32), the values of $T_{2,i}$ are calculated.
3. The procedure of step 2 is repeated for the different subgratings and finally with the aid of Eq. (26) the values of T_i obtained.

3. Numerical results

In this section, numerical results for the angular responses of the different diffracted orders that propagate in holograms with attenuated profiles are presented. To make the theoretical simulations a gratings with a spatial frequency of 500 lines/mm was studied. In order to make the theoretical simulations as realistic as possible the grating was assumed to be embedded between air and glass. The average refractive indices chosen for the theoretical simulations were: $n_a = 1$, $n_p = 1.59$ and $n_v = 1.53$ for air, polymer and glass, respectively. The wavelength used in the simulations was of 633 nm in air. Since we were interested in diffraction efficiencies measured in air the calculated diffraction efficiencies were multiplied by appropriated Fresnel coefficients in order to take into account the interface glass–air, so the diffraction efficiencies measured in air were finally calculated. The number of orders retained in the calculations was of 21: 0, ± 1, ± 2, ± 3,..., although it is important to say that there were no difference observed if only seven orders are used for the thickness used in the simulations, 80 μm. For such high thickness also the RCWT method for a grating without attenuation was proved to converge rapidly for a few orders assumed. The study was also done for the different Bragg conditions, and the angular responses of the efficiency of the different orders centered at each *i*th on-Bragg replay angular condition were calculated.

In order to find the angles of the different orders the so called impact parameter, P, was used [26]. The impact parameter, P, describes whether the hologram is reconstructed in the first, second, third, etc., on-Bragg replay angle condition, P taking the values 1, 2, 3, etc. In the unslanted case the impact parameter is defined as

$$P = \frac{2\beta}{K}\sin(\theta'), \quad (37)$$

where β is the propagation constant inside the medium and θ' is the angle of the incidence wave inside the medium.

It is common in holography to express the profile recorded in the grating in terms of the refractive index. For this study we suppose that a profile of the form

$$n(z) = n_0 + n_1(z)\cos[Kx] + n_2(z)\cos[2Kx] + n_3(z)\cos[3Kx], \quad (38)$$

was stored in the grating, where

$$n_i(z) = n_{i,0}\exp(-\alpha z) \quad \text{for } i = 1,2,3. \tag{39}$$

It is easy to relate the harmonic components of the refractive index to the Fourier components of the dielectric permittivity of Eq. (1), provided that $n_1 \ll n_0$.In this case

$$\varepsilon_{\pm i} = n_0 n_i \quad \text{for } i = 1,2,3. \tag{40}$$

Fig. 2 shows the efficiencies of the ith orders for $i = 0, \pm 1, \pm 2$ and -3 as a function of the angle in air for different values of α and for an unslanted transmission diffraction grating of spatial frequency 500 lines/mm. All the angular responses are centered at the first on-Bragg replay angular condition ($P = 1$). The values used in the theoretical calculations were a thickness of 80 μm and the amplitudes of the three harmonic components of the refractive index were: $n_{1,0} = 0.004$, $n_{2,0} = n_{1,0}/8$, $n_{3,0} = n_{1,0}/20$. These values were assumed for all the theoretical diffraction gratings studied presented here. The reason of using this value of $n_{2,0}$ was in that it has been recently estimated [22] that the ratio between the second and first harmonic components of the refractive index of $n_2/n_1 \sim 7$ is stored in a PVA/acrylamide photopolymer. In all the cases it is clear that the effect of an attenuated profile is to decrease the efficiencies of the different orders propagating in the hologram. An attenuation of the lateral lobes to the main one is also observed in the case of the first and zero order. This can be observed more clearly in Fig. 3 where the efficiency of the first order as a function of the angle of incidence is presented, the efficiency is

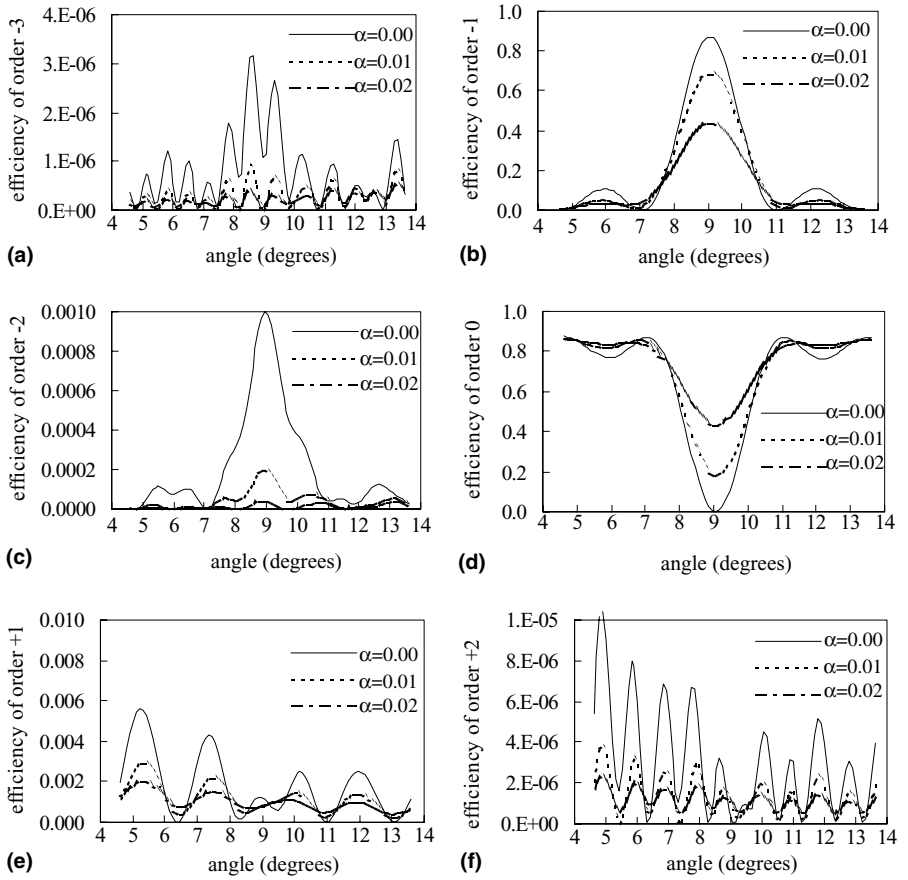

Fig. 2. Efficiency of orders: 0, ±1, ±2, −3 as a function of the angle, centered at first on-Bragg angular replay condition for different values of the attenuation constant α: 0.00, 0.01, 0.02 μm^{-1}, for a spatial frequency of 500 lines/mm. The number of layers was 50.

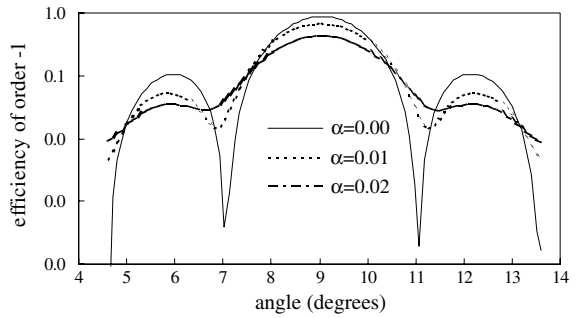

Fig. 3. Efficiency of order −1, as a function of the angle, centered at first on-Bragg angular replay condition for different values of the attenuation constant α: 0.00, 0.01, 0.02 μm^{-1}, for a spatial frequency of 500 lines/mm. The number of layers was 50.

shown in logarithm scale. The effect of the attenuation is to smooth the diffraction efficiency curve. This effect is well-known, Uchida for instance [24], explained it using analytical solutions of the diffraction efficiency of the first order obtained from a two coupled wave method.

Fig. 4 shows the efficiencies of the ith orders for $i = 0, \pm 1, \pm 2, -3$ as a function of the angle in air for different values of α and for a transmission diffraction grating with a spatial frequency of 500 lines/mm. The angular responses centered at the second Bragg angular replay condition ($P = 2$). Fig. 5 shows the efficiency of the second order in logarithmic scale as a function of the angle of in-

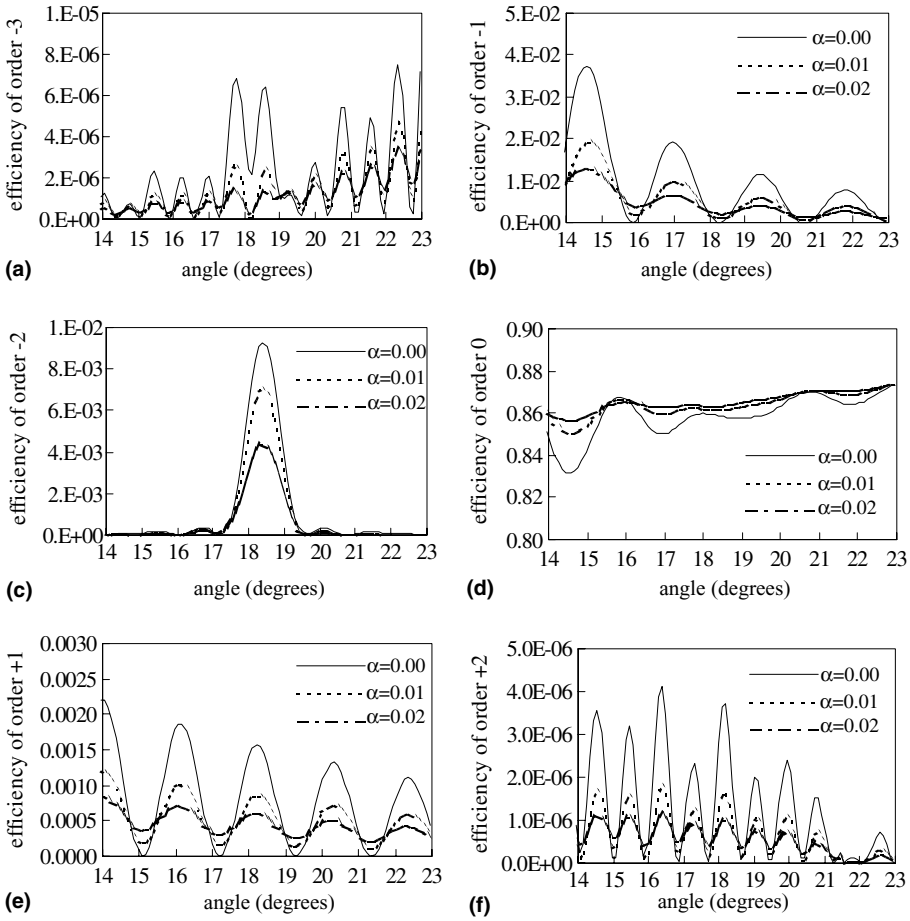

Fig. 4. Efficiency of orders: 0, ± 1, ± 2, -3 as a function of the angle, centered at second on-Bragg angular replay condition for different values of the attenuation constant α: 0.00, 0.01, 0.02 μm^{-1}, for a spatial frequency of 500 lines/mm. The number of layers was 50.

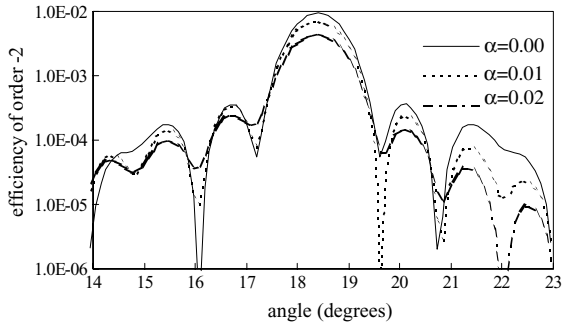

Fig. 5. Efficiency of order −2, as a function of the angle, centered at second on-Bragg angular replay condition for different values of the attenuation constant α: 0.00, 0.01, 0.02 μm^{-1}, for a spatial frequency of 500 lines/mm. The number of layers was 50.

cidence. Again, the effect of the attenuation in the different harmonic components of the refractive index was to smooth the off-Bragg curve.

In Fig. 6 the efficiencies of the ith orders for $i = 0$, ± 1, ± 2, -3 are represented as a function of the angle in air for different values of α and for a transmission diffraction grating with a spatial frequency of 500 lines/mm. The angular responses were centered at the third Bragg angular replay condition ($P = 3$). Fig. 7 presents the efficiency of the third order in logarithm scale. Clearly the same effects observed in previous cases, is observed. Nonetheless, there exist a higher number of lateral lobes to the main one for the efficiency of the third order if compared to the efficiency of the first order. This is due to the fact that the angular selectivity is reduced

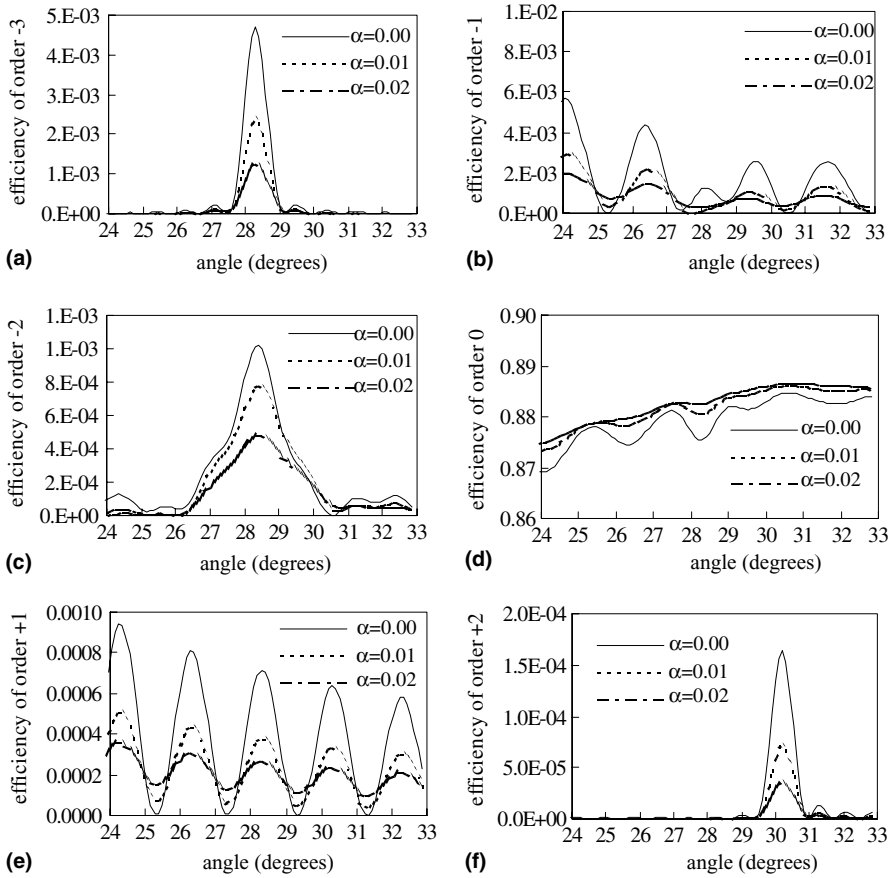

Fig. 6. Efficiency of orders: 0, ± 1, ± 2, -3 as a function of the angle, centered at third on-Bragg angular replay condition for different values of the attenuation constant α: 0.00, 0.01, 0.02 μm^{-1}, for a spatial frequency of 500. The number of layers was 50.

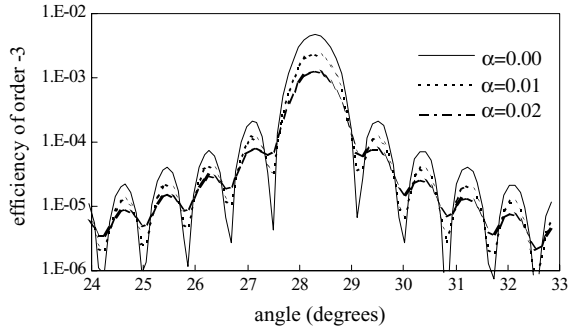

Fig. 7. Efficiency of order −3, as a function of the angle, centered at third on-Bragg angular replay condition for different values of the attenuation constant α: 0.00, 0.01, 0.02 μm^{-1}, for a spatial frequency of 500 lines/mm. The number of layers was 50.

whenever the angular responses are centered at higher Bragg angular replay conditions.

4. Experimental results

In this section we will present the experimental results observed in PVA/acrylamide based photopolymers. The holograms were recorded in PVA/acrylamide photopolymer material using an Argon laser of wavelength 514 nm. The intensity was of 6 mW/cm^2. The beams impinged on the material symmetric to the normal to the recording material, with a beam ratio of 1:1, so unslanted transmission gratings were recorded with $V = 1$. The gratings were recorded with two different spatial frequencies: 545 and 1125 lines/mm. The thickness of the holograms was varied, so as to observe the effects of the attenuation for varying thickness gratings. To prepare the material a method similar to that described in other papers was used [27–29]. A polymerisation solution was prepared using polyvinylalcohol 18-88 (PVA) provided by Fluka as a binder, acrylamide (AA) as monomer and yellowish eosin as dye.

In order to obtain the attenuated refractive index profile we firstly obtained the refractive index modulation as if the grating did not have any attenuation, $n_{1\text{eff}}$

$$n_{1\text{eff}} = \arcsin[(\eta_e/(\eta_e + t_e))^{1/2}]\frac{\lambda\cos\theta'}{\pi d}, \tag{41}$$

where η_e and t_e are the experimentally measured efficiencies of the first and zero order, respectively. The value of η_e was normalized by the sum $(\eta_e t_e)$ in order to correct for losses during reconstruction.

The first order of the refractive index obtained by this way can be considered as an average over the entire thickness as

$$n_{1\text{eff}} = \frac{1}{d}\int_0^d n_{1,0}\exp(-\alpha z)\,dz. \tag{42}$$

So finally it is easy to obtain the value of $n_{1,0}$ related to the values of α and the effective first order of the refractive index $n_{1\text{eff}}$

$$n_{1,0} = n_{1\text{eff}}\frac{\alpha d}{1-\exp(-\alpha d)}. \tag{43}$$

Fig. 8 shows the efficiency of the first order as a function of the reconstruction angle, centered at the first on-Bragg angular replay condition for a transmission diffraction grating with a spatial frequency of 1125 lines/mm. The parameters used for the theoretical simulations of Figs. 8–11 are presented in Table 1. The dots represent the experimental data, whereas the continuous line represents the theoretical simulation. As noted in Section 3 the effect of an attenuated grating is to smooth the off-Bragg responses, in particular the adjacent lobes to the main one are slightly raised if compared to a typical simulation for the diffraction efficiency without attenuation in the refractive index profile. This effect is more critical in Fig. 9

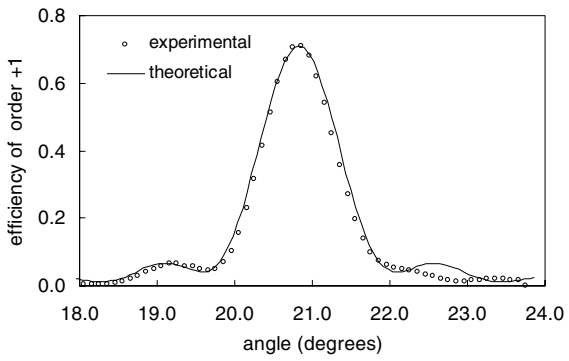

Fig. 8. Efficiency of order +1 as a function of the angle, centered at first on-Bragg angular replay condition a transmission grating recorded on PVA/acrylamide photopolymer with a spatial frequency of 1125 lines/mm and a thickness of 68 μm. The number of layers was 50.

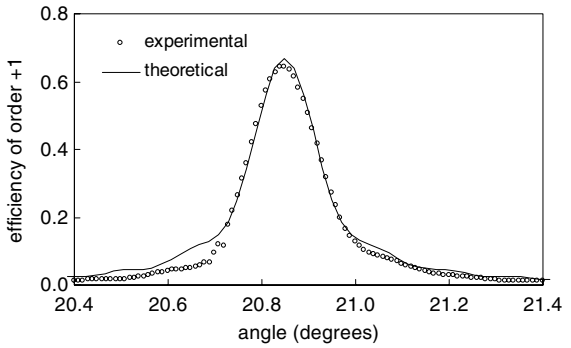

Fig. 9. Efficiency of order +1 as a function of the angle, centered at first on-Bragg angular replay condition a transmission grating recorded on PVA/acrylamide photopolymer with a spatial frequency of 1125 lines/mm and a thickness of 750 μm. The number of layers was 70.

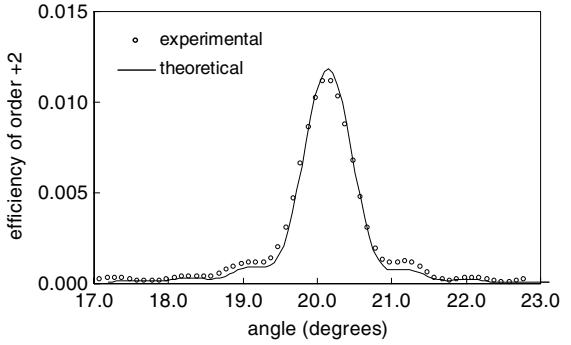

Fig. 10. Efficiency of order +2 as a function of the angle, centered at first on-Bragg angular replay condition a transmission grating recorded on PVA/acrylamide photopolymer with a spatial frequency of 545 lines/mm and a thickness of 117 μm. The number of layers was 50.

where the efficiency of the first order as a function of the reconstruction angle, centered at the first on-Bragg replay angle condition is presented. The grating presented in this figure has the same spatial frequency as that of Fig. 8, but a higher thickness. The thickness of this grating was of 750 μm. The effect of an attenuated grating for this high thickness grating was a clear smoothing of the off-Bragg response curve, so the lateral sidelobe nulls (zeroes) have practically disappeared.

Figs. 10 and 11 present the efficiency of the second order as a function of the reconstruction angle for two diffraction gratings recorded with a

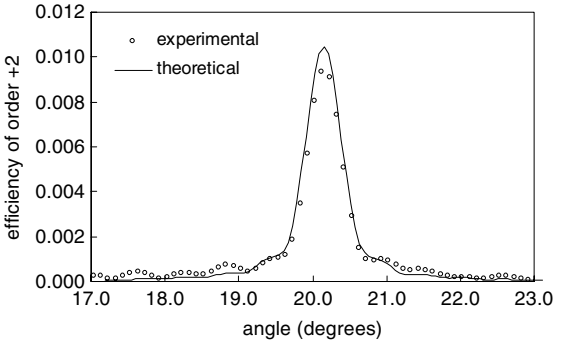

Fig. 11. Efficiency of order +2 as a function of the angle, centered at first on-Bragg angular replay condition a transmission grating recorded on PVA/acrylamide photopolymer with a spatial frequency of 545 lines/mm and a thickness of 160 μm. The number of layers was 50.

Table 1
Values of parameters α, $n_{1,0}$, $n_{2,0}$, d used in the theoretical simulations for transmission diffraction gratings recorded on PVA/acrylamide photopolymers

	Fig. 8	Fig. 9	Fig. 10	Fig. 11
$n_{1,0}$	0.0062	0.0013	0.0037	0.0031
$n_{2,0}$	0	0	0.0006	0.0006
d (μm)	68	750	117	160
α (μm^{-1})	0.020	0.005	0.018	0.016

spatial frequency of 545 lines/mm. The angular response was centered at the second on-Bragg replay angular condition. The gratings have different thickness, that of Fig. 10 presented a thickness of 117 μm, whereas the diffraction grating of Fig. 11 presented a higher thickness, 160 μm. In both cases there is good agreement between the theory and the experiment. It is also interesting to comment that in both cases a second harmonic component of the refractive index was stored in the hologram. The ratio of the second to the first harmonic component of the refractive index was found to be of $\sim$1/7 in both cases.

5. Conclusions

The effects of an attenuated grating profile on the angular responses of the efficiency of the dif-

ferent orders that propagate inside the hologram have been presented. In general the smoothing in the off-Bragg response curves demonstrated by Uchida for the first order has also found in the higher orders. The experimental data presented for the angular responses of the first and also of the second order centered at first and second on-Bragg angular replay condition, demonstrated that an attenuated refractive index profile is stored in volume gratings recorded in PVA/acrylamide photopolymer materials. This attenuation in the profile must be taken into account in models that attempt to explain the mechanism of hologram formation in photopolymer materials.

Acknowledgements

This work was supported by the Ministerio de Ciencia y Tecnología, CICYT, Spain, under project MAT2000-1361-C04-04. 04 and by the "Oficina de Ciencia y Tecnología" (Generalitat Valenciana, Spain) under project GV01-130.

References

[1] M.G. Moharam, T.K. Gaylord, J. Opt. Soc. Am. 71 (1981) 811.
[2] M.G. Moharam, T.K. Gaylord, J. Opt. Soc. Am. 73 (1983) 451.
[3] M.G. Moharam, T.K. Gaylord, J. Opt. Soc. Am. 73 (1983) 1105.
[4] T.K. Gaylord, M.G. Moharam, Proc. IEE 73 (1985) 894.
[5] M.G. Moharam, T.K. Gaylord, J. Opt. Soc. Am. A 3 (1986) 1780.
[6] M.G. Moharam, E.B. Grann, D.A. Pommet, T.K. Gaylord, J. Opt. Soc. Am. A 12 (1995) 1068.
[7] N. Kamiya, Appl. Opt. 37 (1998) 5843.
[8] N.Y. Chang, C.J. Juo, J. Opt. Soc. Am. A 18 (2001) 2491.
[9] P. Dansas, N. Paraire, J. Opt. Soc. Am. A 15 (1998) 1586.
[10] G. Zhao, P. Mouroulis, J. Mod. Opt. 41 (1994) 1929.
[11] S. Piazzolla, B. Jenkins, Opt. Lett. 21 (1996) 1075.
[12] V.L. Colvin, R.G. Larson, A.L. Harris, M.L. Schilling, J. Appl. Phys. 81 (1997) 5913.
[13] I. Aubrecht, M. Miler, I. Koudela, J. Mod. Opt. 45 (1998) 1465.
[14] J.H. Kwon, H.C. Chang, K.C. Woo, J. Opt. Soc. Am. B 16 (1999) 1651.
[15] G.M. Karpov, V.V. Obukhovsky, T.N. Smirnova, V.V. Lemeshko, Opt. Commum. 174 (2000) 391.
[16] J.T. Sheridan, J.R. Lawrence, J. Opt. Soc. Am. A 17 (2000) 1108.
[17] J.T. Sheridan, M. Downey, F.T. O'Neill, J. Opt. A: Pure Appl. Opt. 3 (2001) 477.
[18] J.R. Lawrence, F.T. O'Neill, J.T. Sheridan, J. Opt. Soc. Am. B 19 (2002) 621.
[19] C. Neipp, S. Gallego, M. Ortuño, A. Márquez, M. Álvarez, A. Beléndez, I. Pascual, J. Opt. Am. B 20 (2003) 2052.
[20] H. Kogelnik, Bell Syst. Tech. J. 48 (1969) 2909.
[21] S. Wu, E.N. Glytsis, J. Opt. Soc. Am. B 20 (2003) 1177.
[22] C. Neipp, A. Beléndez, S. Gallego, M. Ortuño, I. Pascual, J.T. Sheridan, Opt. Exp. 11 (2003) 1835.
[23] S. Blaya, L. Carretero, R.F. Madrigal, A. Fimia, Appl. Phys. B 74 (2002) 243.
[24] N. Uchida, J. Opt. Soc. Am 63 (1972) 280.
[25] E.N. Glytsis, T.K. Gaylord, J. Opt. Soc. Am A 4 (1987) 2061.
[26] R.R.A. Syms, Practical Volume Holography, Clarendon Press, Oxford, 1990.
[27] S. Blaya, L. Carretero, R. Mallavia, A. Fimia, M. Ulibarrena, D. Levy, Appl. Opt. 37 (1998) 7604.
[28] C. García, A. Fimia, I. Pascual, Appl. Phys. B 72 (2001) 311.
[29] S. Gallego, M. Ortuño, C. Neipp, C. García, A. Beléndez, I. Pascual, Opt. Exp. 11 (2003) 181.